Depth-Penetrating Temperature Measurements of Thermal Barrier Coatings Incorporating Thermographic Phosphors

Jeffrey I. Eldridge and Timothy J. Bencic, NASA Glenn Research Center, Cleveland, OH 44135;
Stephen W. Allison and David L. Beshears, Oak Ridge National Laboratory, Oak Ridge, TN 37831

Keywords: Thermal barrier boatings, Thermographic phosphors, Temperature measurement

ABSTRACT

Thermographic phosphors have been previously demonstrated to provide effective non-contact, emissivity-independent surface temperature measurements. Because of the translucent nature of thermal barrier coatings (TBCs), thermographic-phosphor-based temperature measurements can be extended beyond the surface to provide depth-selective temperature measurements by incorporating the thermographic phosphor layer at the depth where the temperature measurement is desired. In this paper, thermographic phosphor (Y_2O_3:Eu) fluorescence decay time measurements are demonstrated to provide through-the-coating-thickness temperature readings up to 1100°C with the phosphor layer residing beneath a 100-μm-thick TBC (plasma-sprayed 8wt% yttria-stabilized zirconia). With an appropriately chosen excitation wavelength and detection configuration, it is shown that sufficient phosphor emission is generated to provide effective temperature measurements, despite the attenuation of both the excitation and emission intensities by the overlying TBC. This depth-penetrating temperature measurement capability should prove particularly useful for TBC diagnostics where a large thermal gradient is typically present across the TBC thickness. The fluorescence decay from the Y_2O_3:Eu layer exhibited both an initial short-term exponential rise and a longer-term exponential decay. The rise time constant was demonstrated to provide better temperature indication below 500°C while the decay time constant was a better indicator at higher temperatures.

1. Introduction

Thermal barrier coatings (TBCs) provide highly beneficial thermal protection for turbine engine components (ref. 1). TBCs are ceramic oxide coatings with low thermal conductivity; the most widely used TBC for turbine engine applications is composed of 8wt% yttria-stabilized zirconia (8YSZ). The measurement of temperature gradients through the TBC is critical to the evaluation of TBC performance and health monitoring as well as to the accurate simulation of thermal gradients in engine environments. Non-contact surface temperature measurements of translucent TBCs in a flame environment have proven difficult (ref. 2). For example, the application of infrared (IR) pyrometry to TBCs in an engine environment is problematic because of (1) the interference of reflected radiation and (2) because the TBC translucency at conventional pyrometer wavelengths allows radiation from well below the TBC surface to reach the pyrometer so that surface-specific temperature measurements cannot be obtained. Two approaches have been pursued to surmount these difficulties. One successful approach has been to develop long-wavelength (> 10 μm) pyrometers that operate at wavelengths where the TBCs are opaque (to allow surface measurements) and the TBCs exhibit near-zero reflectance (to minimize interference of reflected radiation), but with the drawback of much lower signal and sensitivity than at shorter wavelengths (refs. 3,4). Another successful approach has been to apply thermographic phosphors to the TBC surface to obtain emissivity-independent surface temperature measurements either by the temperature dependence of the fluorescence decay time or of the ratio of intensities of selected emission lines (refs. 5,6).

One aspect of the potential for using thermographic phosphors for TBC temperature measurements that has not been well explored is to take advantage of the TBC translucency to place the phosphor not only

at the surface, but at any depth where the temperature measurement is desired. The primary obstacle to depth-penetrating measurements is the attenuation of the excitation and emission intensities by the overlying TBC. In particular, YSZ-based TBCs are opaque to the ultraviolet (UV) excitation wavelengths that are normally used for surface temperature measurements. UV excitation of a thermographic phosphor layer has been previously employed for sub-surface temperature measurements; however, the depth penetration allowed by this approach is extremely limited (ref. 7). In this paper, it is demonstrated that with an appropriately chosen excitation wavelength and detection configuration, sufficient phosphor emission is generated to achieve through-the-thickness temperature readings up to 1100°C with the phosphor located beneath a 100-μm-thick TBC. With further development, the strategic placement of luminescent species through the TBC could add embedded sensing functions to the TBC so that the photon-excited emission would provide information about temperature gradients and coating integrity.

2.Strategy for Depth-Penetrating Temperature Measurements

The strategy for achieving depth-probing temperature measurements using thermographic phosphors is to select a phosphor that exhibits significant excitation and emission peaks that can be transmitted through the TBC. The most severe aspect of this limitation is to find a phosphor with an excitation peak at sufficiently long wavelengths, since most phosphors are most efficiently excited at UV wavelengths that will not penetrate into the TBC. Figure 1 illustrates the wavelength restriction presented by the overlying TBC by showing the spectral hemispherical transmittance curve for a 115-μm-thick freestanding plasma-sprayed 8YSZ (PS-8YSZ) coating. This curve shows that there is no transmittance at UV wavelengths (below 380 nm) and that an excitation wavelength above 500 nm is preferred to

achieve transmittances of more than a few percent. As shown in Figure 1, the europia-doped yttria (Y_2O_3:Eu) phosphor has been found to meet this requirement with a minor excitation peak at 532 nm as well as an emission peak at 611 nm. While Y_2O_3:Eu has a much more intense excitation peak at 267 nm and is most effectively excited by a 266 nm fourth harmonic YAG:Nd laser (refs. 6,8), the 532 nm excitation provides a small, but rare significant excitation at a wavelength where the TBC is reasonably transparent. Fortuitously, the 532 nm excitation can be supplied by a second harmonic YAG:Nd laser. While the Y_2O_3:Eu phosphor was used for all the experiments reported in this paper, it should be noted that additional measurements have shown that europia-doped YSZ (YSZ:Eu) also exhibits a minor excitation peak at 532 nm. As reported by Feist and Heyes (ref. 6), YSZ:Eu also functions as an effective thermographic phosphor and provides the additional advantage of being the same composition as the TBC itself except for the introduction of the low-level doping with europia, and therefore should be more compatible than a completely distinct phosphor layer.

3. Experimental Procedure

3.1 Coatings

The plasma-sprayed 8YSZ (PS-8YSZ) TBC specimens were prepared by plasma-spraying 8YSZ powder (Zircoa, Inc.) onto sacrificial carbon disks (25.4 mm diameter x 3.2 mm thick). The estimated TBC thickness was 100 μm. The Y_2O_3:Eu phosphor layer was painted onto the TBC surface using a 50:50 mixture (by volume) of HPC and LK (ZYP Coatings, Inc.) water-based binders. The paint containing approximately 20% Y_2O_3:Eu (6% Eu) powder by volume was applied to the TBC-coated carbon disks using a standard airbrush. The thickness of the applied phosphor paint was estimated to be approximately 25 μm. Specimens were subsequently heated in air at 800°C to set the binder and to burn

off the carbon substrate. The final freestanding specimens could then be oriented with the phosphor layer positioned either above or below the TBC.

3.2 Luminescence Spectroscopy and Decay Time Measurements

A Renishaw System 2000 Raman microscope was adapted to acquire both luminescence spectra and fluorescence decay time measurements. Figure 2 shows a simplified schematic of this Raman-microscope-based system in which the following adaptations were made: (1) the original 514 nm continuous Ar ion laser was replaced by a low-power (4 μJ/pulse) Nanogreen (model, NG-00321-110, JDS Uniphase) pulsed (5.2 kHz) 532 nm YAG:Nd laser to enable pulsed excitation, (2) a 532 nm longpass edge filter replaced the 514 nm notch filter, and (3) a photomultiplier tube (PMT; Hamamatsu Model HC125-01) was installed behind the angle-tunable filter wheel to detect the time-resolved fluorescence; the time-resolved fluorescence signal was collected by a 100 MHz digital oscilloscope (Agilent model 54622A) external to the spectrometer that was triggered by the laser pulse. The specimen was mounted in a hot stage (Linkam Model TS1500) attached to the stage of an optical microscope equipped with a 20x ultra-long working distance objective (Mitutoyo). The laser was defocused to a diameter of approximately 100 μm to provide relative insensitivity to local inhomogeneities in the coating. With this configuration (Fig. 2), the phosphor layer emission spectra as a function of temperature were acquired with the translatable diverting mirror removed from the optical path so that the dispersion created by the grating is resolved by the position-sensitive (but not time-resolved) CCD detector. Without any realignment, refocusing, or sample repositioning, the fluorescence decay time measurements were acquired with the translatable mirror positioned to divert the optical path towards the filter wheel and PMT. For high spectral resolution, the narrow bandpass (< 1 nm) angle-tunable filter

could then be positioned to select any of the emission peaks observed in the phosphor emission spectra. However, the high-resolution narrow bandpass filters that were originally in the filter wheel of the Renishaw 2000 Raman Microscope only transmitted a small fraction of the Y_2O_3:Eu emission peak, which becomes quite broad at high temperatures. Therefore, for improved signal-to-noise, a wide bandpass filter (FWHM = 10 nm) centered at 610 nm was used for the measurements reported here. In addition, to maximize signal-to-noise, the triggered decay-time measurements were averaged over 16384 laser pulses. In addition, a blank run with no excitation laser was run at each temperature to provide a baseline correction.

3.3 Fluorescence Decay Time Analysis

Inspection of the fluorescence decay curves for the primary 611 nm emission peak produced by the Y_2O_3:Eu phosphor (Figure 3) indicated that the decay curves could not be modeled by a simple exponential decay and that modeling should incorporate a rise time as well as a decay time. This observation is consistent with the report of a temperature- and dopant-level-dependent rise time for the 611 nm emission in Y_2O_3:Eu by Ranson et al. (ref. 9). The rise time was attributed to the relatively sluggish energy transfer between nearby Eu^{3+} ions sitting at inequivalent Y^{3+} symmetry sites (from $^5D_1$ level of $Eu^{3+}(C_{3i})$ to the $^5D_0$ level of $Eu^{3+}(C_2)$). The simple model proposed by Ranson et al. (ref. 9) to incorporate this slower energy transfer between inequivalent sites into the fluorescence decay behavior, $I_{emission}(t)$, was adopted here:

$$I_{emission}(t) = [c_1 + c_2[1 - e^{\frac{-t}{\tau_{rise}}}]]e^{\frac{-t}{\tau_{decay}}} \qquad (1)$$

where $I_{emission}(t)$ is the emission intensity as a function of time, c_1 and c_2 are scaling constants, and τ_{rise} and τ_{decay} are the rise time and decay time, respectively. The rise time, decay time, and two scaling constants were determined by fitting Equation 1 to the decay-time measurements using the Solver utility in Microsoft Excel. Figure 3 shows a curve that was fit to the data in this manner.

4. Results

The temperature dependence of the emission spectra from the Y_2O_3:Eu layer (on top of the TBC) is shown in Figure 4. For comparison, the spectra were normalized to display similar maximum intensities; actual signals decreased significantly at higher temperatures. The prominent 611 nm emission peak shows a small but consistent displacement to longer wavelengths as well as a significant broadening with increasing temperature. By fitting these peaks to a mixed Gaussian-Lorentzian peak shape, the changes in peak position and width can be examined more quantitatively by plotting the emission peak position and full width at half maximum (FWHM) as a function of temperature (Figure 5). Both the peak position and FWHM show a consistent, nearly linear increase with increasing temperature. The temperature dependence of the emission peak position and FWHM suggests the possibility of using this temperature dependence to perform temperature measurements. However, these peak parameters are also likely to show a significant stress dependence (useful for stress monitoring (ref. 10)) that may interfere with accurate temperature measurements. Fluorescence decay measurements were selected as better suited for temperature measurements due to their higher temperature sensitivity and relative lack of stress dependence.

Figure 6 shows that the intensity of the observed 611 nm emission (room temperature) from the Y_2O_3:Eu layer is reduced considerably (factor of ~30) when the phosphor layer is below the 100-μm thick TBC compared to when the phosphor layer is above the TBC. This reduction is due to the attenuation of both the 532 nm excitation and the 611 nm emission intensities (see Fig. 1). However, even with this significant reduction, the 611 nm emission from the phosphor below the TBC was still easily detected and the reduced intensity was sufficient to perform fluorescence decay time measurements.

Fluorescence decay time measurements were performed for both orientations of the freestanding coatings: with the Y_2O_3:Eu phosphor layer above the TBC and with the phosphor layer below the TBC. For each orientation, decay time measurements were performed as a function of coating temperature. Measurements were obtained at 50°C intervals up to 600°C and then at 20°C intervals up to 1100°C. The hot stage was held at each selected temperature for a minimum of 10 min before decay time measurements were acquired. Both τ_{decay} and τ_{rise} were determined by fitting Equation 1 to the fluorescence decay data and values of τ_{decay} are displayed in Figure 7. The resulting plot shows that there was a good match between the values determined for the Y_2O_3:Eu layer above the TBC and the values determined for the Y_2O_3:Eu layer beneath the TBC, indicating that the temperature calibrations of the fluorescence decay time are equivalent and that despite the signal attenuation due to the overlying TBC, the phosphor layer located below the TBC still functions as an effective temperature probe.

Figure 7 also shows that τ_{decay} is relatively insensitive to temperature at temperatures below 500°C and therefore does not provide an effective temperature probe at these lower temperatures. However, Figure 8 shows that τ_{rise} has a significantly higher sensitivity to temperature below 500°C and offers the potential of providing temperature indication in this range. Above 500°C, the much greater temperature sensitivity of τ_{decay} "kicks in" and makes τ_{decay} a much better temperature indicator than τ_{rise}. Also, above 800°C, within the limitations of the instrumentation used here, τ_{rise} becomes too short to determine accurately.

5. Measurement Capability

While Figure 7 demonstrates the successful application of a Y_2O_3:Eu phosphor layer for through-the-thickness TBC temperature measurements up to 1100°C, TBCs are subjected to temperatures up to 1200°C in current turbine engine designs, and future generations of TBCs will be required to sustain even higher temperatures. To achieve these higher temperature measurements, further optimization of the fluorescence decay measurements will be required. Measurements above 1100°C proved difficult because the fluorescence intensity decreases dramatically with increasing temperature resulting in poor signal-to-noise ratio and the decay time becomes very short (< 1 μsec). The loss in fluorescence signal intensity could be offset through use of a pulsed laser with higher power pulses than the very low power (4 μJ/pulse) laser used for this paper; several orders of magnitude increase in signal could easily be achieved through a higher power laser.

Another difficulty in extending thermographic-phosphor-based temperature measurements to higher temperatures arises from an increased thermal radiation background that is superimposed onto the light generated by the phosphor emission. It was found that the microscope-based light collection configuration employed for this report excelled in minimizing the thermal radiation background in the fluorescence decay measurements. Even at 1000°C, the thermal radiation background was a negligible contribution to the fluorescence decay measurements (in contrast to the emission spectra where the thermal radiation background was quite noticeable (Fig. 4)). This suppression of thermal radiation background is proposed to be due to the microscope-based configuration that restricts collection of thermal radiation to a small area around the excitation laser spot.

Finally, thermographic-phosphor-based temperature measurements may interfere with the TBC performance (bonding, lifetime, and thermal protection) when a distinct Y_2O_3:Eu phosphor layer is inserted into the TBC/substrate system. For retaining TBC performance, a much more acceptable solution would be to introduce layered low-level doping of Eu into the 8YSZ material of which the TBC is composed. As previously noted, this approach should succeed since YSZ:Eu has been demonstrated to be an effective thermographic phosphor (ref. 6).

6. Summary

The use of thermographic phosphor (Y_2O_3:Eu) fluorescence decay time measurements were demonstrated for through-the-thickness temperature readings up to 1100°C with the phosphor layer residing beneath a 100-μm thick freestanding PS-8YSZ TBC. These depth-penetrating temperature measurements were accomplished by selecting a phosphor, Y_2O_3:Eu, that has a minor excitation peak at

532 nm and emission peak at 611 nm that could all be transmitted through the TBC. In particular, switching from the commonly used excitation peak at 267 nm (where the TBC is opaque) to the excitation peak at 532 nm allows sufficient transmittance of the excitation wavelength. The adaptation of a Raman microscope was found to be especially convenient for sequentially obtaining phosphor layer emission spectra as a function of temperature and then to use these spectra to select emission peaks for performing fluorescence decay-time measurements with the same instrument. Successful temperature measurements were performed up to 1100°C with the phosphor layer underneath a 100-μm thick TBC despite attenuation of the detected fluorescence intensity by a factor of ~30 due to the overlying TBC. The temperature calibration of fluorescence decay times for the phosphor layer below the TBC was equivalent to the calibration for the phosphor layer above the TBC. While the decay time, τ_{decay}, provided the best temperature indication above 500°C, the rise time, τ_{rise}, was a better indicator below 500°C.

In conclusion, the successful demonstration of the use of thermographic phosphors to achieve depth-penetrating temperature measurements shows significant potential for the incorporation of luminescent species into TBCs to add sensing functions that will provide information about temperature gradients and coating integrity.

References

1. D. Zhu and R.A. Miller, Thermal-Barrier Coatings for Advanced Gas-Turbine Engines," MRS Bull., 2000, 25(7), pp.43-47.

2. K.W. Tobin, S.W. Allison, M.R. Cates, G.J. Capps, D.L. Beshears, M. Cyr, and B.W. Noel, "High-Temperature Phosphor Thermometry of Rotating Turbine Blades," AIAA J., 1990, 28(8), pp. 1485-1490.
3. J.R. Markham and K. Kinsella, "Thermal Radiative Properties and Temperature Measurement from Turbine Coatings," Int. J. Thermophysics, 1998, 19(2), pp. 537-545.
4. H. Latvakoski, J. Markham, M. Borden, T. Hawkins, and M. Cybulsky, "Measurement of Advanced Ceramic Coated Superalloys with a Long Wavelength Pyrometer," AIAA Report 2000-2212, American Institute of Aeronautics, 21st AIAA Aerodynamic Measurement Technology and Ground Testing Conference, June 2000, Denver, CO.
5. S.W. Allison, D.L. Beshears, M.R. Cates, B.W. Noel, and W.D. Turley, "Taking an Engine's Temperature,", Mech. Eng., 1997, 119(1), pp. 72-74.
6. J.P. Feist and A.L. Heyes, "Development of the Phosphor Thermometry Technique for Applications in Gas Turbines," 10th International Symposium on Applications of Laser Techniques to Fluid Mechanics, Lisbon, Portugal, 2000.
7. K.L. Choy, J. Mei, J.P. Feist, and A.L. Heyes, "Microstructrue and Thermoluminescence Properties of ESAVD Produced Eu Doped Y2O3-ZrO2 Coatings," Surface Eng., 2000, 16(6), pp. 469-72.
8. S. D. Alaruri, A.J. Brewington, M.A. Thomas, and J.A. Miller, "High-Temperature Remote Thermometry Using Laser-Induced Fluorescence Decay Lifetime Measurements of Y_2O_3:Eu and YAG:Tb Thermographic Phosphors," IEEE Trans. Instrum. Measurement, 1993, 42(3), pp. 735-39.
9. R.M. Ranson, E. Evangelou, and C.B. Thomas, "Modeling the Fluorescent Lifetime of Y_2O_3:Eu," Appl. Phys. Lett., 1998. 72(21), pp. 2663-2664.

10. X. Peng and D.R. Clarke, "Piezospectroscopic Analysis of Interface Debonding in Thermal Barrier Coatings," J. Amer. Ceram. Soc., 2000, 83(5), pp. 1165-70.

Figure Captions

Figure 1. Hemispherical transmittance plot for a 115-μm-thick freestanding PS-8YSZ TBC along with excitation and emission spectra for Y_2O_3:Eu.

Figure 2. Schematic of Raman-microscope-based system used to acquire both phosphor layer emission spectra and fluorescence decay time measurements as a function of coating temperature.

Figure 3. Fluorescence decay curve at 700°C from Y_2O_3:Eu layer beneath freestanding 100-μm thick PS-8YSZ (gray). The black curve is the result of fitting Equation 1 to the data.

Figure 4. Emission spectra as a function of temperature for Y_2O_3:Eu layer above freestanding 100-μm thick PS-8YSZ TBC.

Figure 5. Peak position and FWHM of 611 nm emission peak from Y_2O_3:Eu phosphor layer as a function of temperature.

Figure 6. Comparison of 611 nm emission intensity at room temperature for Y_2O_3:Eu layer above versus below freestanding 100-μm thick PS-8YSZ TBC. Emission spectrum for Y_2O_3:Eu below the TBC was multiplied x10 for easier comparison.

Figure 7. Decay time (τ_{decay}) as a function of coating temperature for Y_2O_3:Eu layer above versus below freestanding 100-μm thick PS-8YSZ TBC.

Figure 8. Comparison of decay time (τ_{decay}) versus rise time (τ_{rise}) as a function of temperature determined from decay of 611 nm emission from Y_2O_3:Eu layer.

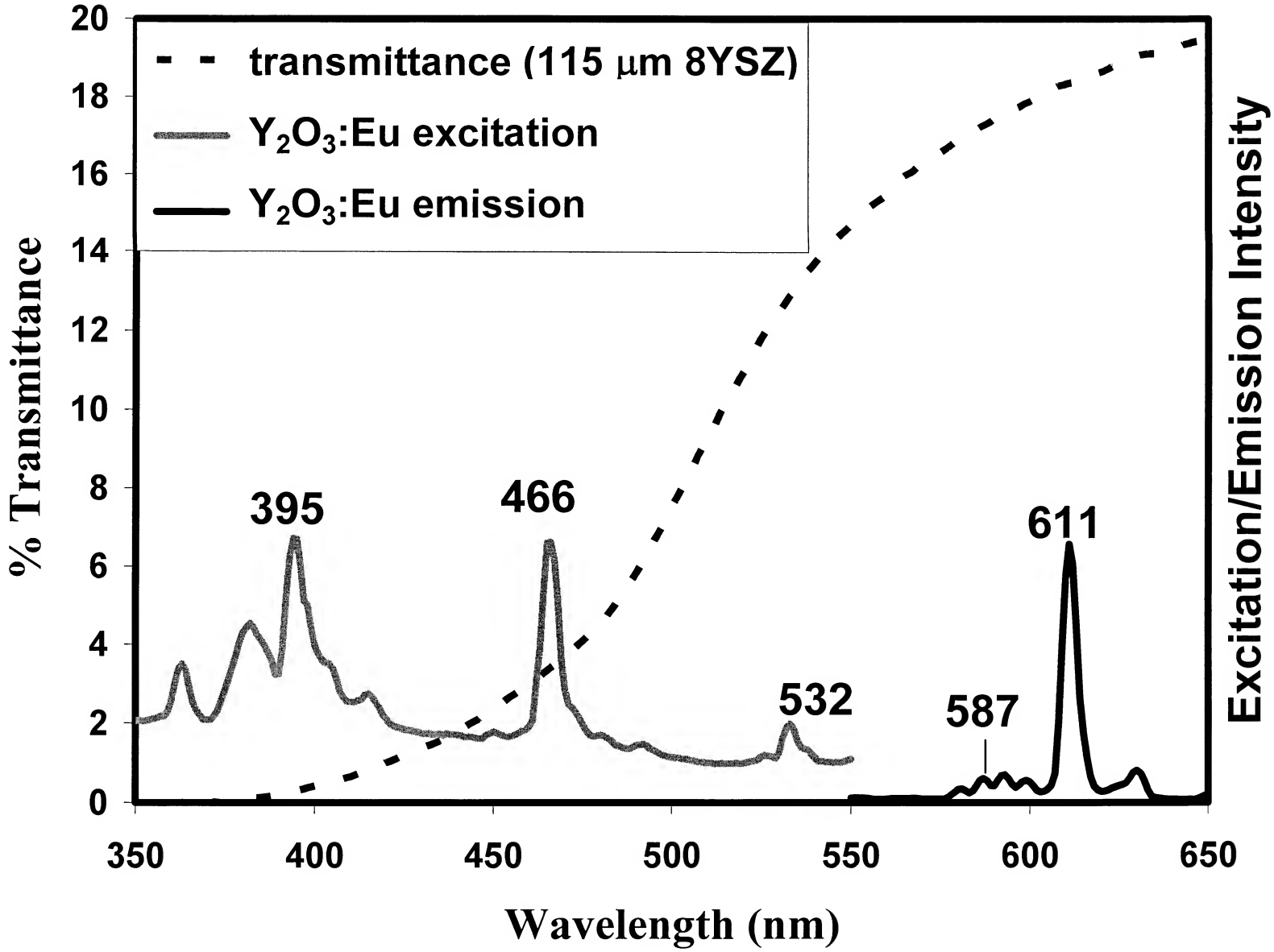

Figure 1. Hemispherical transmittance plot for a 115-μm-thick freestanding PS-8YSZ TBC along with excitation and emission spectra for Y_2O_3:Eu.

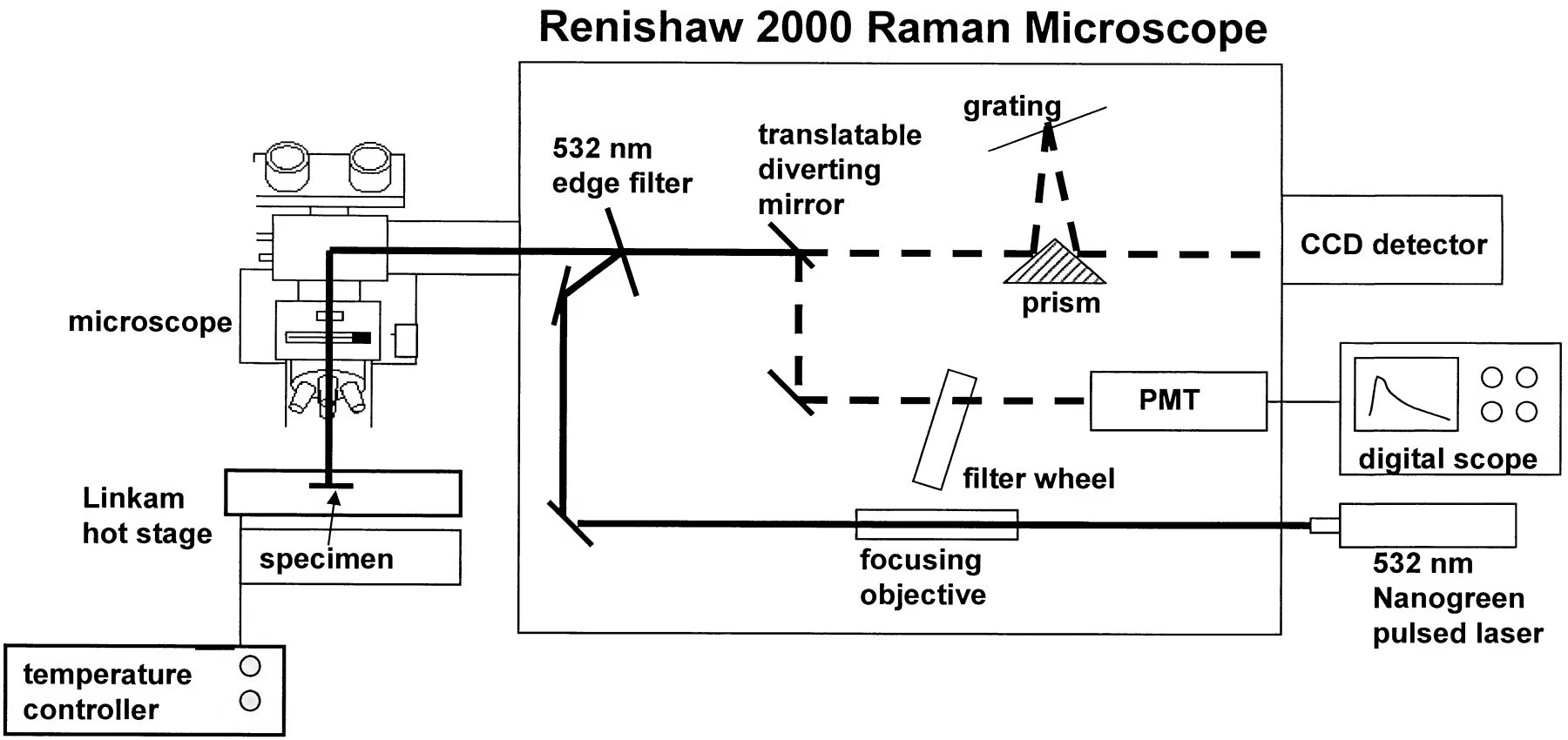

Figure 2. Schematic of Raman-microscope-based system used to acquire both phosphor layer emission spectra and fluorescence decay time measurements as a function of coating temperature.

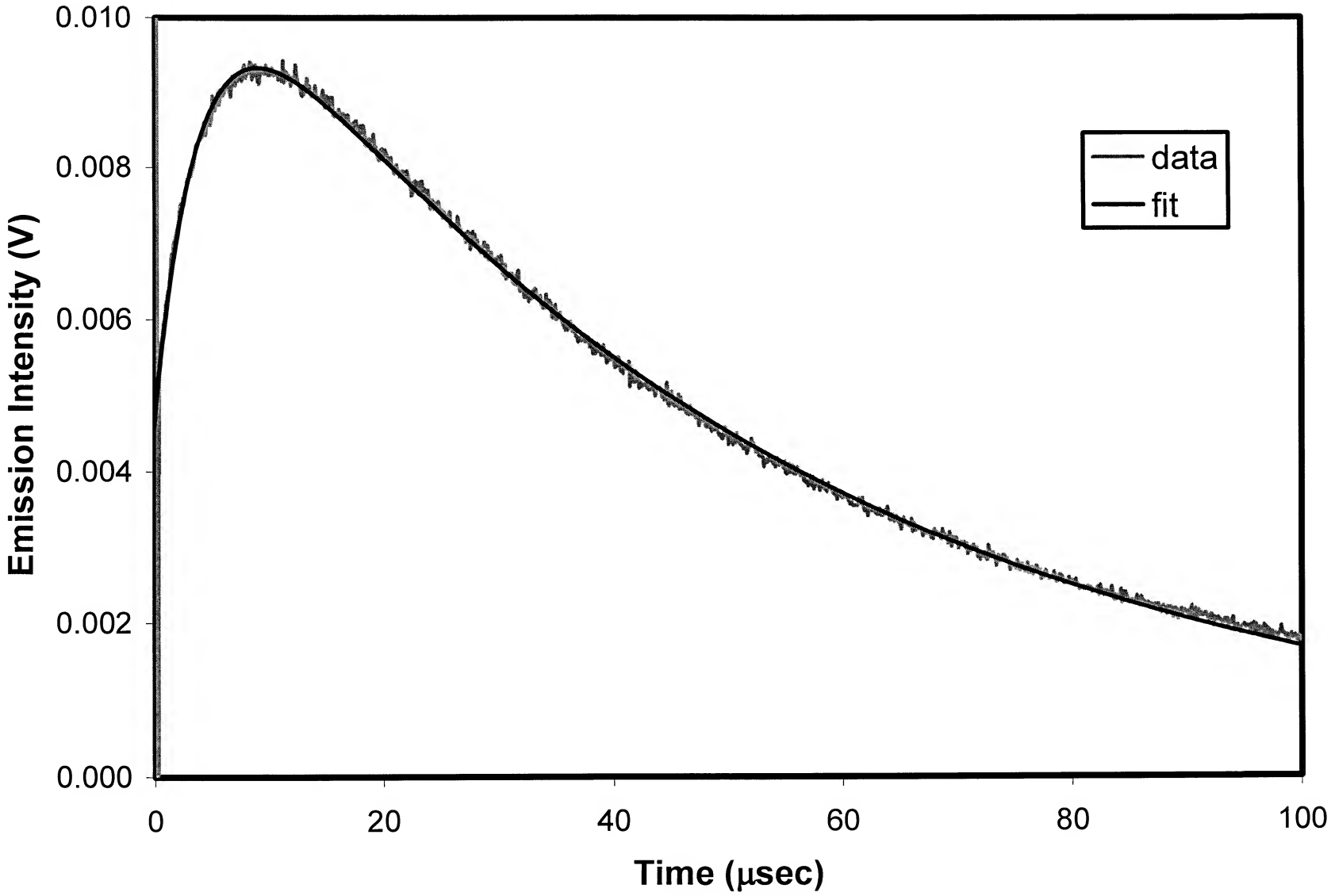

Figure 3. Fluorescence decay curve at 700°C from Y_2O_3:Eu layer beneath freestanding 100-μm thick PS-8YSZ (gray). The black curve is the result of fitting Equation 1 to the data.

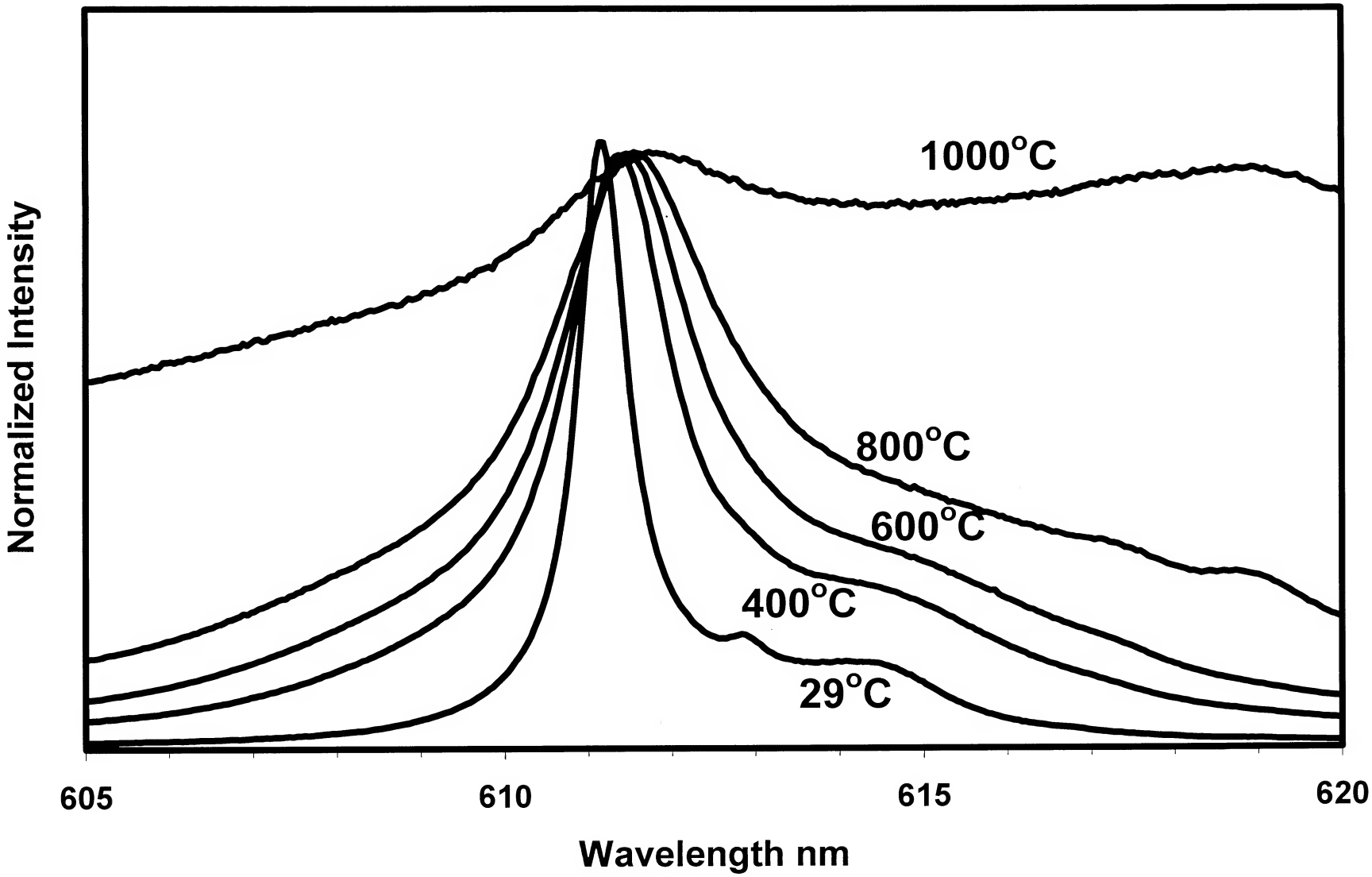

Figure 4. Emission spectra as a function of temperature for Y_2O_3:Eu layer above freestanding 100-μm thick PS-8YSZ TBC.

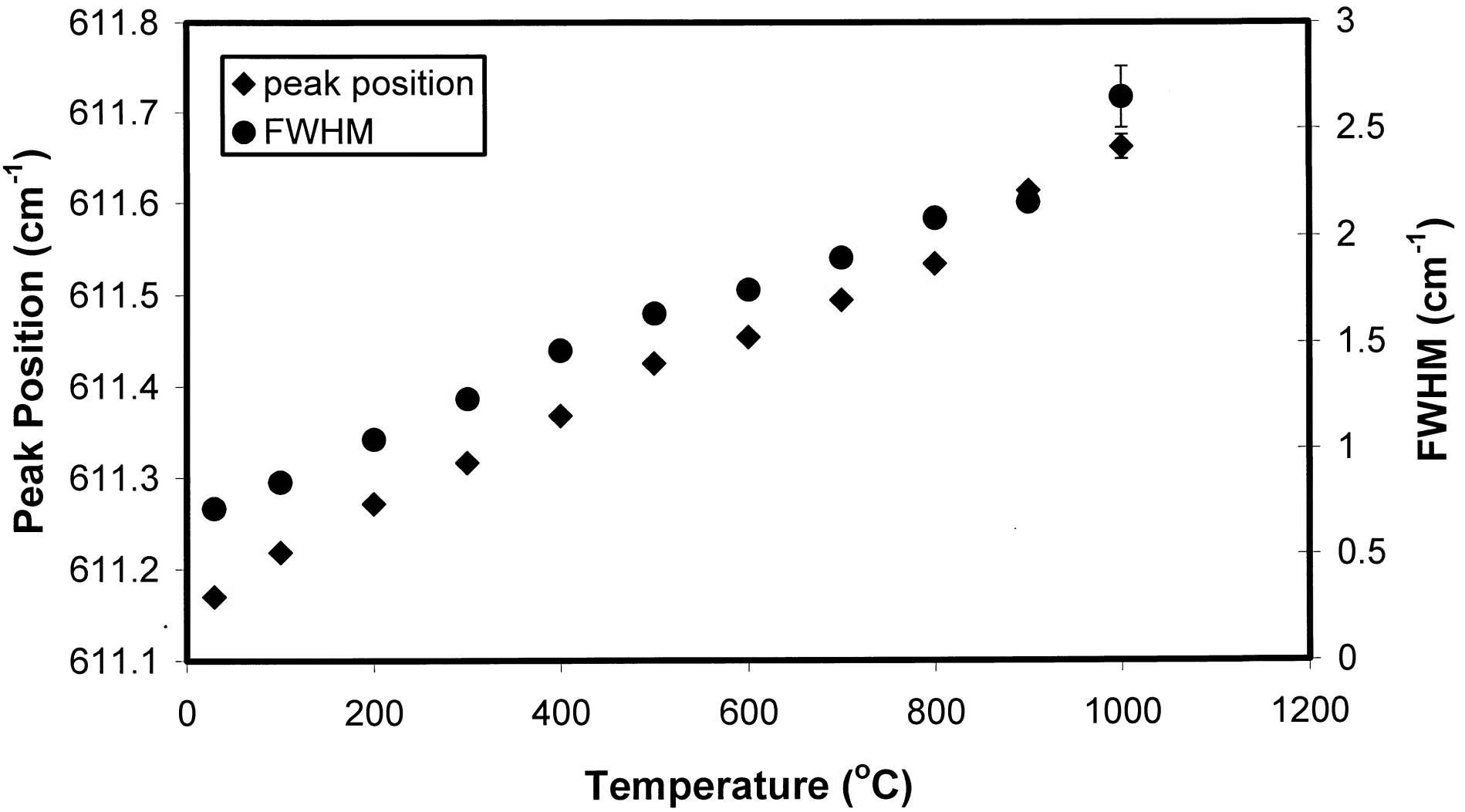

Figure 5. Peak position and FWHM of 611 nm emission peak from Y_2O_3:Eu phosphor layer as a function of temperature.

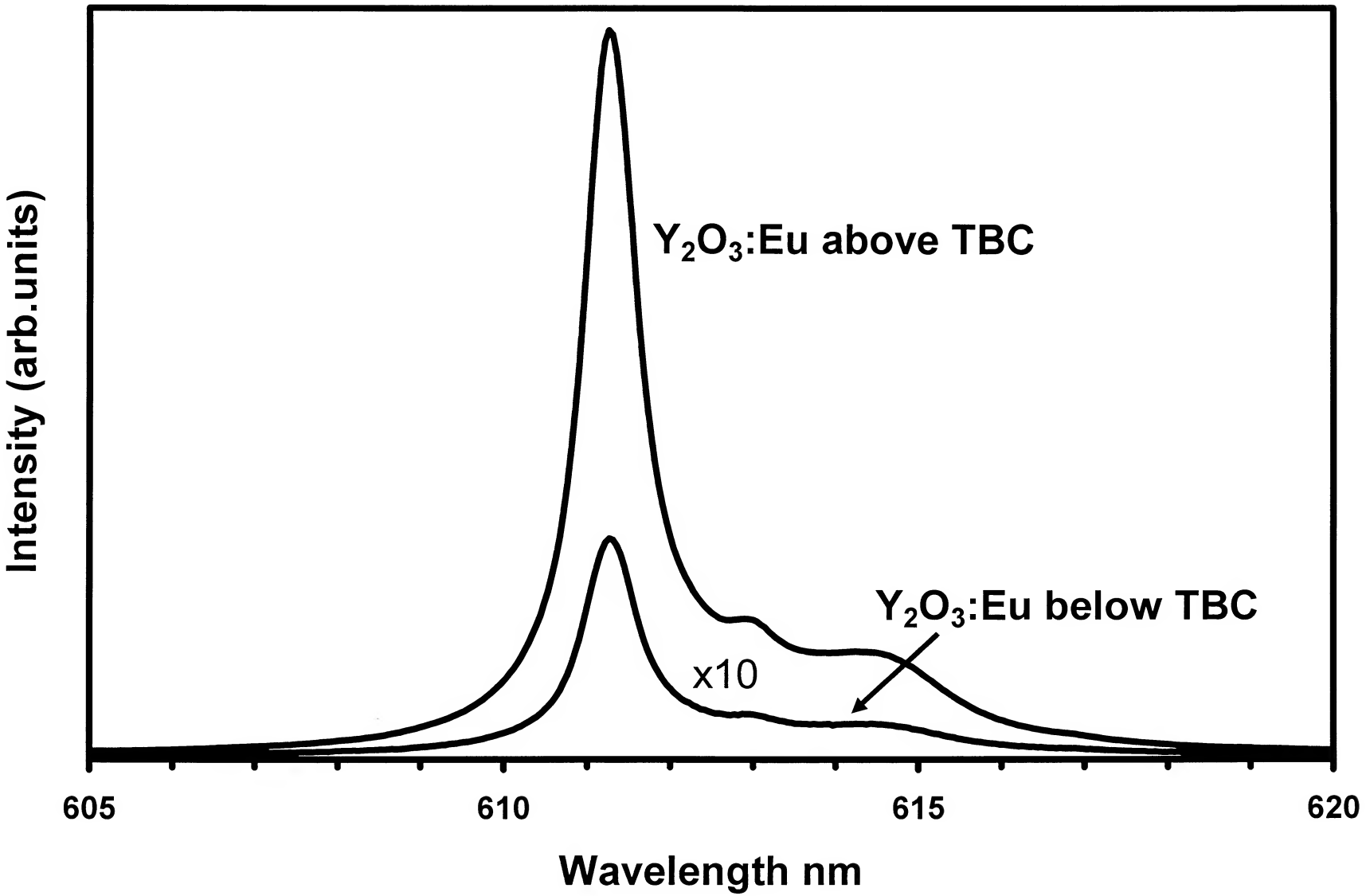

Figure 6. Comparison of 611 nm emission intensity at room temperature for Y_2O_3:Eu layer above versus below freestanding 100-μm thick PS-8YSZ TBC. Emission spectrum for Y_2O_3:Eu below the TBC was multiplied x10 for easier comparison.

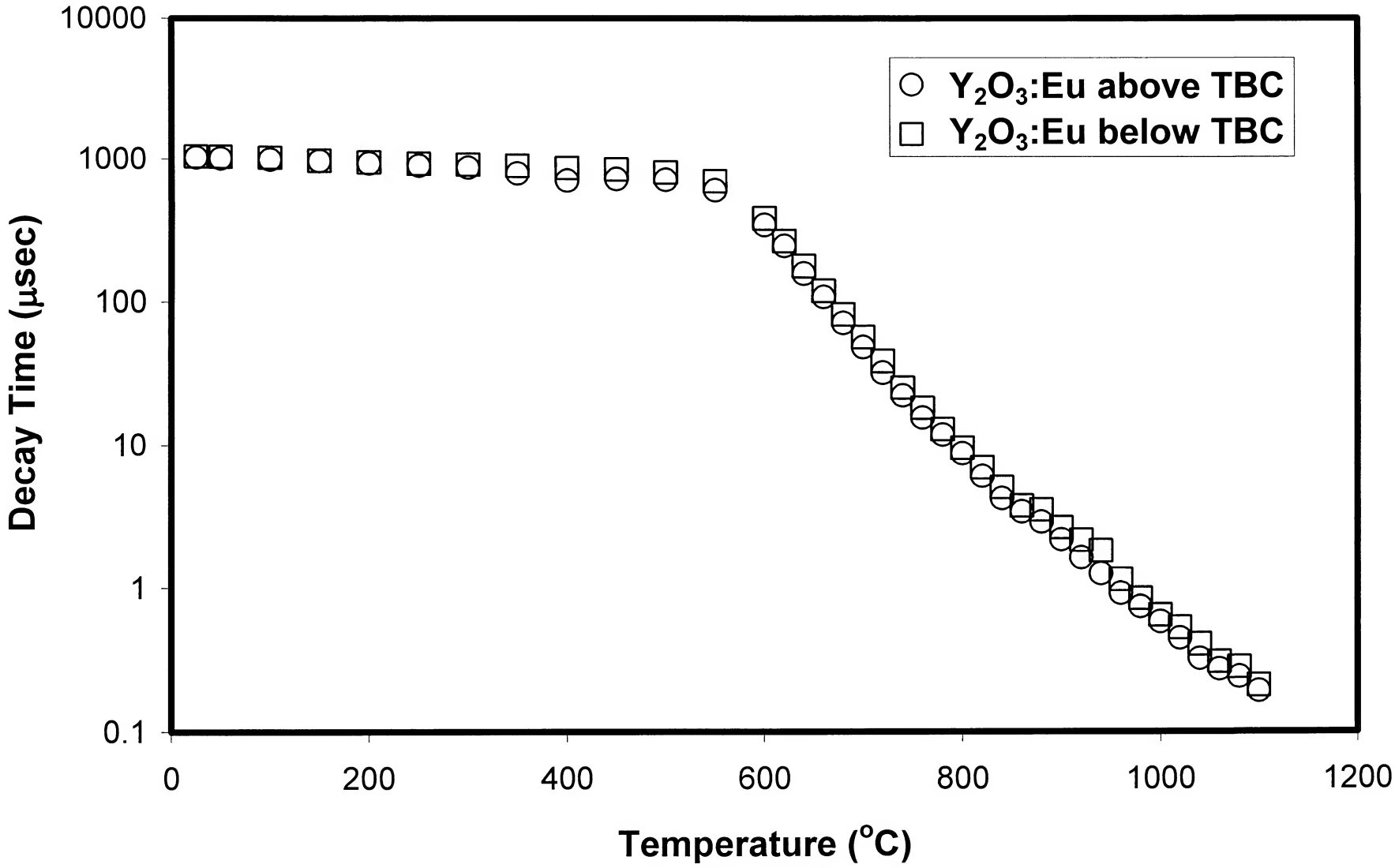

Figure 7. Decay time (τ_{decay}) as a function of coating temperature for Y_2O_3:Eu layer above versus below freestanding 100-µm thick PS-8YSZ TBC.

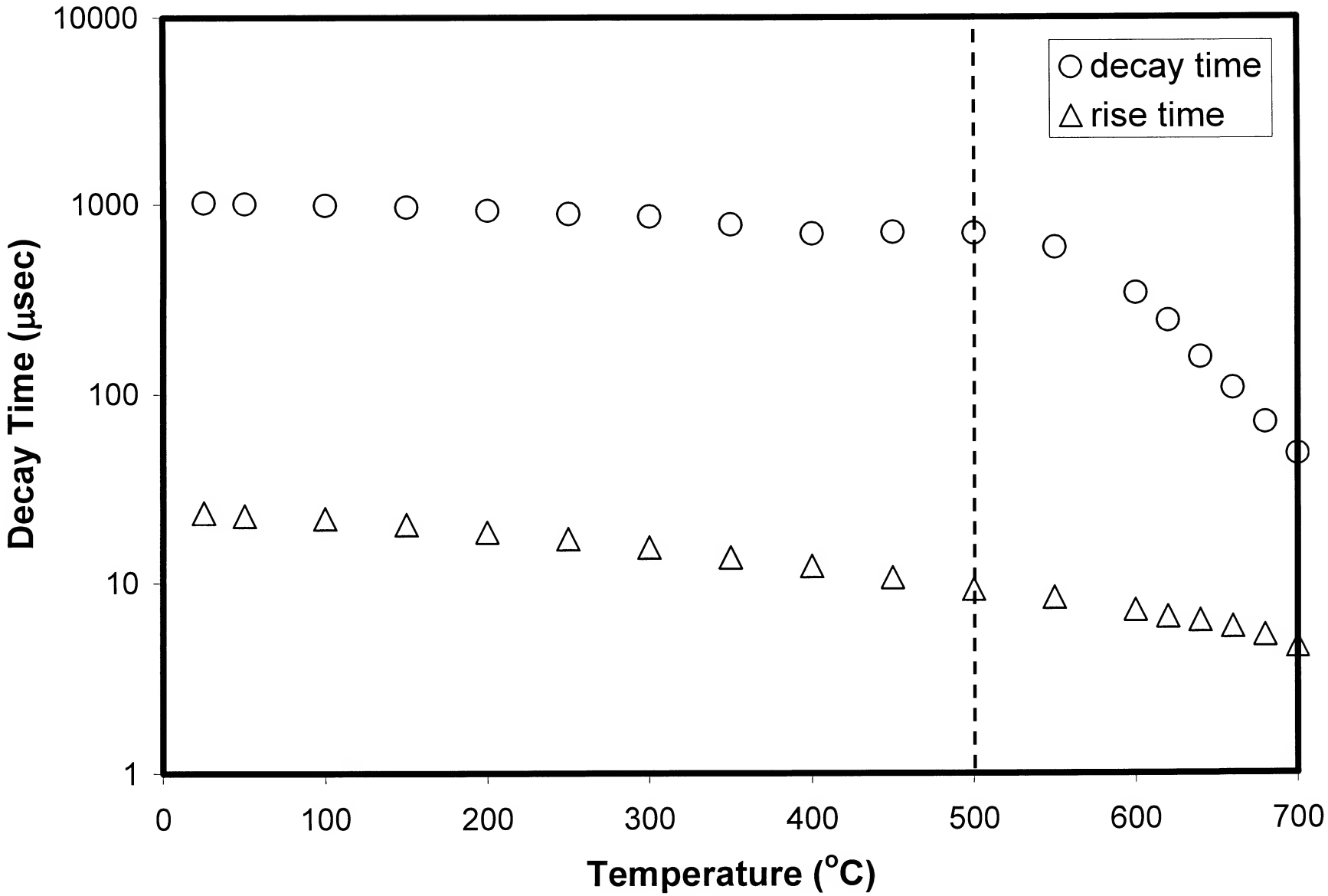

Figure 8. Comparison of decay time (τ_{decay}) versus rise time (τ_{rise}) as a function of temperature determined from decay of 611 nm emission from Y_2O_3:Eu layer.